

Polysulfide regulation by zwitterionic barrier towards durable lithium-sulfur batteries

Gaoran Li, Fei Lu, Xiaoyuan Dou, Xin Wang, Dan Luo, Hao Sun, Aiping Yu, and Zhongwei Chen

J. Am. Chem. Soc., **Just Accepted Manuscript** • DOI: 10.1021/jacs.9b13303 • Publication Date (Web): 29 Jan 2020

Downloaded from pubs.acs.org on January 30, 2020

Just Accepted

“Just Accepted” manuscripts have been peer-reviewed and accepted for publication. They are posted online prior to technical editing, formatting for publication and author proofing. The American Chemical Society provides “Just Accepted” as a service to the research community to expedite the dissemination of scientific material as soon as possible after acceptance. “Just Accepted” manuscripts appear in full in PDF format accompanied by an HTML abstract. “Just Accepted” manuscripts have been fully peer reviewed, but should not be considered the official version of record. They are citable by the Digital Object Identifier (DOI®). “Just Accepted” is an optional service offered to authors. Therefore, the “Just Accepted” Web site may not include all articles that will be published in the journal. After a manuscript is technically edited and formatted, it will be removed from the “Just Accepted” Web site and published as an ASAP article. Note that technical editing may introduce minor changes to the manuscript text and/or graphics which could affect content, and all legal disclaimers and ethical guidelines that apply to the journal pertain. ACS cannot be held responsible for errors or consequences arising from the use of information contained in these “Just Accepted” manuscripts.

Polysulfide regulation by zwitterionic barrier towards durable lithium-sulfur batteries

Gaoran Li,¹ Fei Lu,^{1,2} Xiaoyuan Dou,¹ Xin Wang,^{3*} Dan Luo,¹ Hao Sun,⁴ Aiping Yu,¹ Zhongwei Chen^{1*}

¹ Department of Chemical Engineering, Waterloo Institute of Nanotechnology, University of Waterloo, 200 University Avenue West, Waterloo, ON N2L 3G1 Canada

² College of Chemistry, Chemical Engineering and Materials Science, Shandong Normal University, Jinan 250014, P. R. China

³ International Academy of Optoelectronics at Zhaoqing, South China Academy of Advanced Optoelectronics, South China Normal University, Guangdong 510631, China

⁴ Institute of Functional Material Chemistry, Faculty of Chemistry, National & Local United Engineering Lab for Power Battery, Northeast Normal University, Renmin Street 5268, Changchun, Jilin 130024, People's Republic of China

ABSTRACT: Rational regulation on polysulfide behaviors is of great significance in pursuit of reliable solution-based lithium-sulfur (Li-S) battery chemistry. Herein, we develop a unique polymeric zwitterion (PZI) to establish a smart polysulfide regulation in Li-S batteries. The zwitterionic nature of PZI integrates sulfophilicity and lithiophilicity in the matrix, fostering an ionic environment for selective ion transfer through the chemical interactions with lithium polysulfides (LiPS). When implemented as a functional interlayer in cell configuration, PZI empowers strong obstruction against polysulfide permeation but simultaneously allows fast Li⁺ conduction, thus contributing to significant shuttle inhibition as well as the resultantly facile and stable sulfur electrochemistry. The PZI-based cells realize excellent cyclability over 1000 cycles with a minimum capacity fading rate of 0.012 % per cycle and favorable rate capability up to 5 C. Moreover, high areal capacity retention of 5.3 mAh cm⁻² after 300 cycles can be also obtained under raised sulfur loading and limited electrolyte, demonstrating a great promise in developing high-efficiency and long-lasting Li-S batteries.

INTRODUCTION

Lithium-sulfur (Li-S) batteries present one of the most promising solutions to high-efficiency and cost-effective energy storage.¹⁻³ Yet despite their intriguing virtues such as high energy density and low cost, the fulfillment of reliable sulfur electrochemistry is perplexed by several intractable challenges that give rise to unsatisfactory practical capacity and cyclability.^{4,5} Among them, the “shuttle effect” epitomizes the most distinguishing characteristic of Li-S batteries as compared to conventional Li-ion chemistries. Triggered by their strong solvation in ether-based electrolyte, the highly mobile lithium polysulfides (LiPS) perform continuous round-trip diffusion between cathode and anode along with their chemical and electrochemical participations in both electrode reactions, leading to severe sulfur loss, electrode passivation and coulombic inefficiency.⁶⁻⁸

Targeting this issue, aggressive strategies have been proposed capable of completely eliminating the polysulfide shuttling through the employment of non-solvating electrolyte or rigorous spatial/covalent-constraint sulfur electrodes, which contribute to the “solid-based” instead of the conventional “solution-based” sulfur electrochemical reaction mechanism.⁹⁻¹¹ While the merits of stability and safety are convincing, solid sulfur electrochemistry suffers from sluggish electron/ion transfers with resultant kinetic degradation, and is still in its early infancy struggling with energy inefficiency, cost issue, and industrial compatibility.^{12,13} In this respect, the solution-based counterpart involves sulfur solid-liquid phase conversions and chemical equilibriums, leading to continuous exposure of electron/ion-accessible interfaces and uniformization of sulfur distribution.¹⁴⁻¹⁶ As a result, the solution-based sulfur electrochemistry is more accessible to superior sulfur utilization, rate capability and energy density, as well as favorable scalability and compatibility to current battery industry for near-future commercial implementations.¹⁷⁻¹⁹ Nevertheless, rational polysulfide regulation that fosters these strengths and circumvents the detrimental shuttle effect is requisite for the success of solution-based Li-S batteries.

1
2
3
4
5
6
7
8
9
10
11
12
13
14
15
16
17
18
19
20
21
22
23
24
25
26
27
28
29
30
31
32
33
34
35
36
37
38
39
40
41
42
43
44
45
46
47
48
49
50
51
52
53
54
55
56
57
58
59
60

Considering that the shuttle effect originates from the dual behaviors, i.e., dissolution and diffusion of polysulfides, selective regulation that allows the dissolution but resists the diffusion behavior could serve as an ideal approach to managing the advantages and disadvantages of solution-based sulfur electrochemistry. Following this concept, the construction of functional interlayer between cathode and separator emerges as the most pertinent countermeasure and attracts intense research enthusiasm worldwide.^{20,21} The rationale behind this strategy lies in the interactive behaviors between interlayer materials and polysulfides, which can be generally classified into two categories, i.e., adsorbing and repelling mechanisms. The former employs multifarious adsorbents such as carbon materials, polar inorganics, and their composites, to physically or chemically capture and reuse sulfur species, so as to enhance sulfur utilization and simultaneously suppress their migration.²²⁻²⁴ However, the adsorbing interlayers generally suffer from limited adsorbability and porous architecture, which degrade the polysulfide-blocking effect particularly under low-adsorbent-dosage and high-sulfur-loading conditions. As for the latter mechanism, the interlayers are specifically designed to chemically/electrostatically repel the polysulfide anions and restrain the active species within the cathode, which can be represented by functional polymers such as Nafion and inorganics such as VOPO₄.^{25,26} These designs deliver good capability of sulfur confinement due to the ion selective instincts, yet are still haunted by the sluggish Li⁺ conduction in the dense blocking matrix with a resultant deterioration in redox kinetics. Therefore, the establishment of advanced interlayer that concurrently fulfills efficient polysulfide blockage and facile Li⁺ transfer remains challenging but significant in pursuit of reliable solution-based sulfur electrochemistry.

In this contribution, a unique polymeric zwitterion (PZI) was developed for rational polysulfide regulation in Li-S batteries. Prepared by a facile and highly processible copolymerization, the PZI combines sulfophilic and lithiophilic moieties by covalently tethering the imidazolium cation and sulfonate anion within the alkyl- and alkoxy-based matrix. The interactive chemistry between PZI and LiPS was investigated by a series of experimental and computational characterizations. Polysulfide anions serve as electron donor to be anchored on the imidazole rings, while Li⁺ preferably intimates to the sulfonate

1
2
3 terminals in the polymeric framework, thus contributing to the enhancement of LiPS
4 dissociation, facilitation on Li⁺ conduction and constraint on polysulfide diffusion. When
5 implemented as interlayer, these interactions enable an in-situ formation of polysulfide-
6 concentrated shield that strongly obstructs the polysulfide penetration but simultaneously
7 allows a facile Li⁺ transfer in solution-based Li-S configuration. Attributed to these
8 favorable features, cells based on PZI interlayer realize excellent cyclability with minimum
9 capacity fading rate of 0.012 % per cycle upon long-term 1000 cycles, decent rate
10 capability of 718.4 mAh g⁻¹ at 5 C, and high areal capacity retention of 5.3 mAh cm⁻² after
11 300 cycles at raised sulfur loading and limited electrolyte. These results demonstrate the
12 great superiorities of the as-developed PZI in polysulfide regulation, offering a new
13 pathway towards reliable solution-based sulfur electrochemistry and high-performance Li-
14 S batteries.
15
16
17
18
19
20
21
22
23
24

25 RESULTS AND DISCUSSION

26 **Synthesis and Characterization.** The polymeric zwitterion (PZI) was prepared through a
27 free radical copolymerization process. 3-(1-vinyl-3-imidazolio) propanesulfonate (VIPS)
28 was firstly synthesized via the ionization reaction according to our previous reports (Figure
29 1a).^{27,28} Subsequently, the PZI membrane was obtained by copolymerizing VIPS and
30 poly(ethylene glycol) methyl ether methacrylate (PEGMEM) in a home-made mould with
31 poly(ethyleneglycol) dimethacrylate (PEGDMA) and 2-hydroxy-2-methylpropiophenone
32 as cross-linker and photo-initiator, respectively (Figure 1b, see details in Experimental).
33 Benefiting from the facile and processable fabrication, the PZI membrane can be well
34 controlled in size and thickness. The successful co-polymerization was confirmed by
35 Fourier transform infrared spectroscopy (FTIR) as shown in Figure S1. The disappearance
36 of C=C stretching vibration at 1655 cm⁻¹ confirms the p-bond opening and the addition
37 polymerization to form the alkyl skeleton, while the emergence of new peaks at 1109 and
38 1730 cm⁻¹ corresponding respectively to C-O-C and C=O vibrations verifies the grafting
39 of alkoxy and ester groups in the resultant polymeric matrix.^{29,30} The thermal properties of
40 the obtained PZI were examined by thermogravimetric analysis (TGA) and differential
41 scanning calorimetry (DSC). As shown in Figure S2a, PZI maintains thermally stable till
42 250 °C. Meanwhile, the DSC result reveals a T_g around -50 °C and no observable melting
43
44
45
46
47
48
49
50
51
52
53
54
55
56
57
58
59
60

point for PZI (Figure S2b), which ensures its thermal stability and good ion mobility within regular battery operation temperature range.³¹

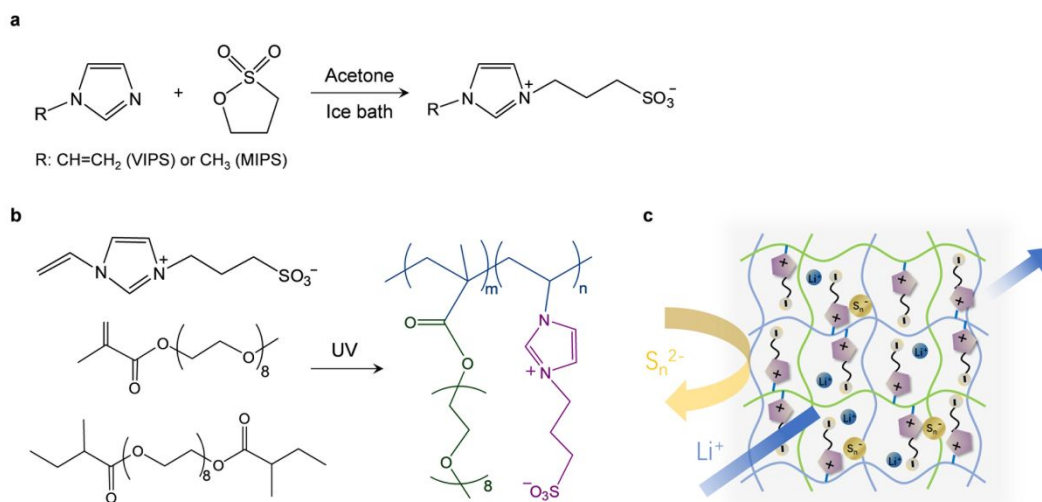


Figure 1. synthesis of (a) MIPS or VIPS, and (b) PZI; (c) schematic illustration of the functional groups and the ion selectiveness of PZI membrane

Figure 1c schematically depicts the functional structures in PZI membrane. The as-developed PZI delivers an alkyl skeleton, which favors a structural robustness with good mechanical and chemical stabilities. Apart from that, the alkoxy chains endow PZI with considerable flexibility as well as good compatibility/wettability to the ether-based electrolyte, which facilitates the Li^+ transfer within the matrix.³² More importantly, the copolymerization establishes unique zwitterionic structures with covalently anchored cationic imidazole rings and anodic sulfonic terminal groups within the PZI network. Zwitterions with covalently tethered ion pairs have been well recognized in regulating specific ion mobility, which provide a unique ionic environment for effectively managing the ion transfer behaviors.³³ Beyond that, zwitterion could also serve as a unique solvent with large dipole moment for enhancing the disassociation of the solute and facilitating the conduction of the target ion.³⁴ In our case, these unique features are designed to impose regulative interactions with LiPS in purpose of a concurrent realization of desirable polysulfide confinement and facile Li^+ conduction in Li-S batteries.

Interactions between zwitterion and LiPS. ^1H NMR and ^7Li NMR spectra were collected in methanol- d_4 solution to investigate the interactions between the zwitterion and LiPS. It

1
2
3 should be noted that all the NMR spectra were collected by using an analogous monomeric
4 structure, i.e., 3-(1-methyl-3-imidazolium) propanesulfonate (MIPS), to represent PZI
5 considering their identical zwitterionic structure (Figure 1) and the poor solubility of PZI
6 in methanol. Meanwhile, Li_2S_4 was employed as the representative LiPS for NMR analysis.
7
8 Figure 2a presents the proton assignment in ^1H NMR spectra. In drastic contrast to pristine
9 MIPS, the $\text{Li}_2\text{S}_4@\text{MIPS}$ composite witnesses a vanishment of the resonance peak assigned
10 to H_a (highlighted in blue background in Figure 2a and amplified in Figure 2b). This
11 variation can be attributed to the incorporation of polysulfide that neutralizes the imidazole
12 ring in MIPS and intensifies the acidity of H_a . Consequently, H_a tends to be deuterated by
13 methanol- d_4 solution, leading to this peak vanishment in the spectrum.³⁵ Moreover, clear
14 upfield shifts can be observed for the resonance peaks of imidazole proton H_b and H_c when
15 MIPS is composited with Li_2S_4 (highlighted in orange background in Figure 2a and
16 amplified in Figure 2c). This could be induced by the electrostatic coupling between
17 cationic imidazole ring and anionic polysulfide, which increases of the electron cloud
18 density of the carbon atoms in imidazolium and accordingly intensifies the shielding
19 effect.³⁶ In addition, the proton in methanol hydroxy (highlighted in green background in
20 Figure 2a and amplified in Figure 2d) undergoes a downfield shift in the $\text{Li}_2\text{S}_4@\text{MIPS}$
21 spectrum due to the formation of “lithium bonding”-like interaction between Li_2S_4 and
22 methanol.³⁷ Figure 2e shows the variation of ^7Li chemical shift before and after composite
23 with zwitterion. With the addition of MIPS, the ^7Li resonance of Li_2S_4 exhibits a downfield
24 shift from -0.114 to -0.082 ppm, suggesting the intensification of shielding effect on Li^+
25 via the possible formation of $\text{SO}_3^- \text{-Li}^+$ pairing.³⁸ Such interaction is expected to facilitate
26 the Li^+ transfer by strengthening the dissociation and ionization of LiPS due to the high
27 donor capability of $-\text{SO}_3^-$ to Li^+ . These results cooperatively demonstrate the strong
28 interactions between the zwitterions and LiPS through the formation of two pairs of cation-
29 anion couples, i.e., imidazole(+)-polysulfide(-) and lithium ion(+)-sulfonate(-),
30 conforming to the electrostatic attractions and Lewis acid-base interaction principles.
31
32
33
34
35
36
37
38
39
40
41
42
43
44
45
46
47
48
49
50
51
52
53
54
55
56
57
58
59
60

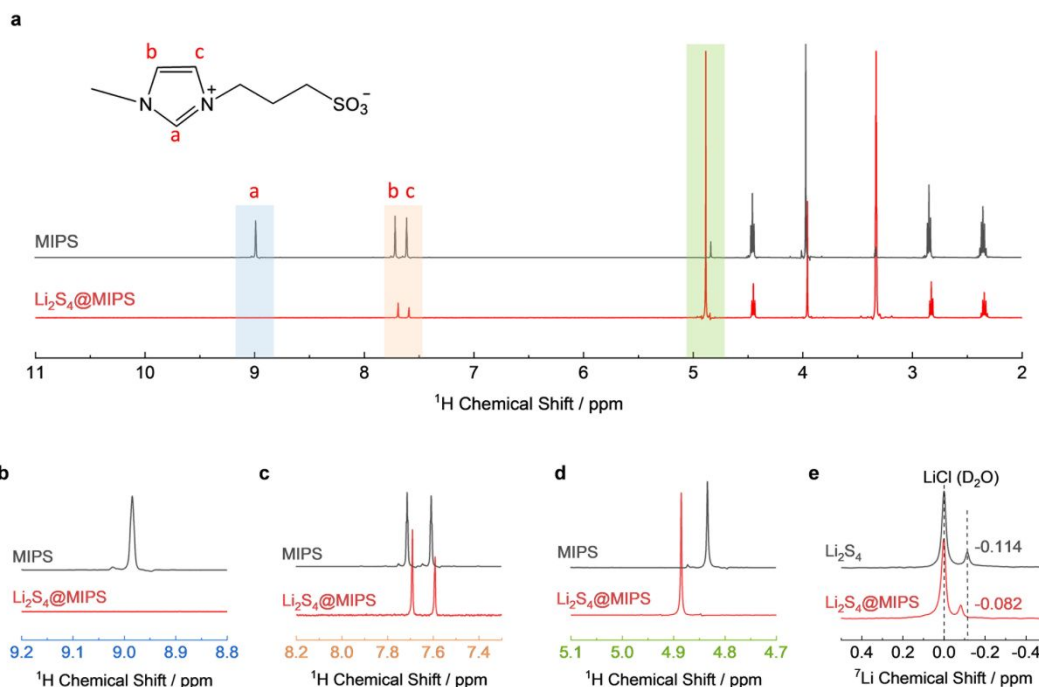


Figure 2. (a) ^1H NMR spectra of MIPS and $\text{Li}_2\text{S}_4@\text{MIPS}$ composite; amplified ^1H NMR spectra of the (b) blue, (c) orange and (d) green regions for MIPS and $\text{Li}_2\text{S}_4@\text{MIPS}$ composite; (e) ^7Li NMR spectra of Li_2S_4 and $\text{Li}_2\text{S}_4@\text{MIPS}$ composite.

The chemical interactions are also supported by FTIR analysis as shown in Figure S3. The $\text{Li}_2\text{S}_4@\text{MIPS}$ composite imposes a significant peak shift for the S=O vibration in MIPS from 1038 to 1061 cm^{-1} , which signifies the coupling between $-\text{SO}_3^-$ and Li^+ in line with the NMR results.^{28,39} Moreover, the peaks assigned to the ring breathing of imidazole (1211 cm^{-1}), C=C (1471 cm^{-1}) and C=N stretching (1576 cm^{-1}) vibrations in MIPS also undergo considerable shifts after composite with Li_2S_4 , suggesting the strong inter-attraction between cationic imidazole and anionic polysulfide.^{40,41} Apart from that, X-ray photoelectron spectroscopy (XPS) analysis was performed to further study the interactive chemistry between zwitterion and LiPS. As shown in Figure 3a, the N 1s spectrum of MIPS shows a single peak at 401.6 eV due to the orbital conjugation on the imidazole ring.⁴² Notably, this peak shifts to a lower binding energy range after composite with Li_2S_4 , indicating the increase of electron cloud density in the imidazole ring due to its coordination with the electron-rich polysulfide anion. The Li 1s spectra of Li_2S_4 and $\text{Li}_2\text{S}_4@\text{MIPS}$ show a consistent peak at 54.6 eV assigned to the Li-S bonding (Figure 3b). However, the $\text{Li}_2\text{S}_4@\text{MIPS}$ composite witnesses a new peak emerging at 55.4 eV attributed

to the formation of Li-O bonding, which further confirms the interaction between Li^+ and $-\text{SO}_3^-$.⁴³ Figure 3c depicts the chemical states of sulfur element in different samples. MIPS shows a typical S 2p spectrum of sulfonate group with two sub peaks locating at 166.6 and 167.8 eV. Meanwhile, Li_2S_4 shows typically two pairs of peaks corresponding to the terminal sulfur (S_T^-) at 161.6 eV and bridging sulfur (S_B^0) at 163.1 eV, respectively.⁴⁴ It is worth noting that these characteristic peaks shift to higher binding energies for the $\text{Li}_2\text{S}_4@\text{MIPS}$ composite ascribed to the coordination between sulfonate and Li^+ as well as polysulfides and imidazolium cation, which decrease the electron cloud density in sulfur.⁴⁵

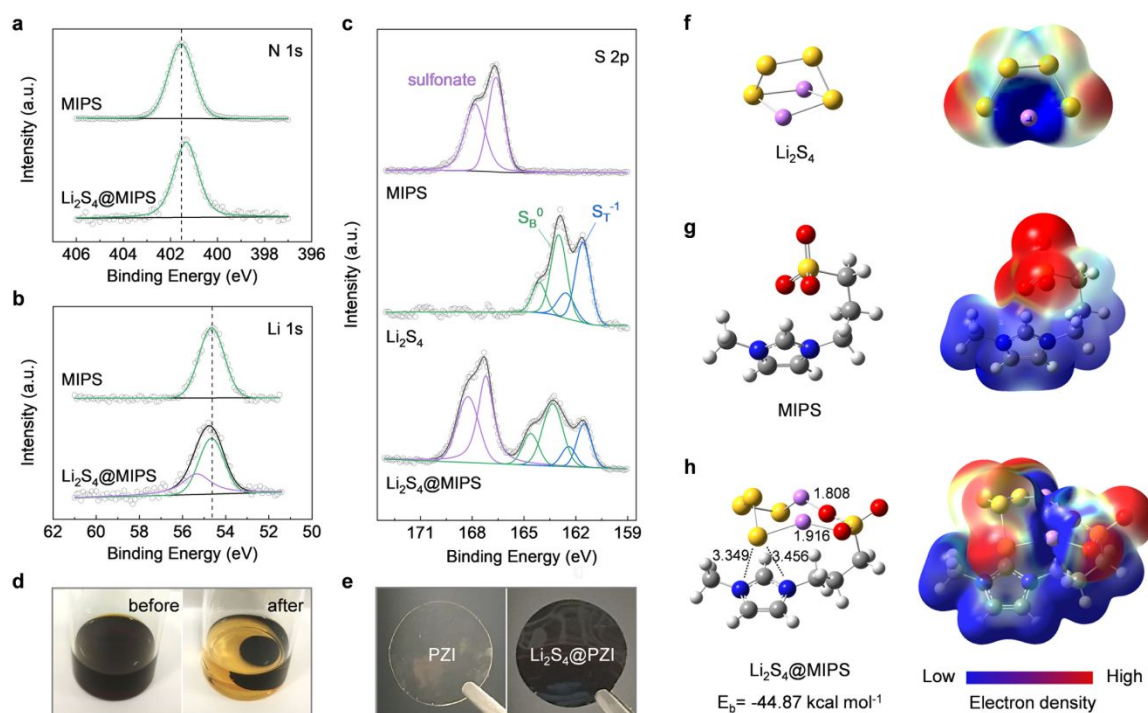


Figure 3. (a) N 1s, (b) Li 1s and (c) S 2p XPS spectra of MIPS, Li_2S_4 and $\text{Li}_2\text{S}_4@\text{MIPS}$ composite; optical images of (d) LiPS solution and (e) PZI membrane before and after adsorption test; geometrically stable configurations (left) and electron density distributions (right) of (f) Li_2S_4 , (g) MIPS and (h) $\text{Li}_2\text{S}_4@\text{MIPS}$ composite.

Given this, the interactions between zwitterion and LiPS was visualized through a direct adsorption characterization by immersing the as-prepared PZI membrane into 0.1 M $\text{Li}_2\text{S}_4/(\text{DME}+\text{DOL})$ solution for 24 hrs. As shown in Figure 3d, the pristine LiPS solution exhibits a typical dark brown color, while a clear and light orange solution was obtained after adsorption by PZI along with the membrane changing from transparent to dark brown

(Figure 3e). This result optically verifies the great LiPS adsorbability of PZI via the strong chemical interactions, which is capable of resisting a considerable concentration gradient as demonstrated by the color contrast between the solution and membrane after adsorption. Beyond these experimental evidences, the interactive behaviors between zwitterion and LiPS were also explored by theoretical calculations. Figure 3f, g and h depict the geometrically stable configurations of Li_2S_4 , MIPS and $\text{Li}_2\text{S}_4@\text{MIPS}$ composite, respectively. The stable composite system can be achieved with the S_4^{2-} anion adsorbed onto the imidazolium cation, while the Li^+ coordinates with the $-\text{SO}_3^-$ terminal through a S-Li-O “lithium bond”-like bridging,³⁷ contributing to a high adsorption energy up to ca. $-44.87 \text{ kcal mol}^{-1}$. The two Li-O bond distances are ca. 1.808 and 1.916 Å, respectively, confirming the formation of Li-O bond in consistent with the XPS result. Meanwhile, the distances between the adjacent S and the N in the imidazole ring are 3.349 and 3.456 Å respectively, which also validates the chemical/electrostatic attraction between the cationic imidazole and anionic polysulfide. These interactive behaviors can be also described by the electron density distribution (Figure 3f-h), where the electron-rich domain (red) couples with the electron-lean domain (blue) following the Lewis acid-base theory. Accordingly, the electron density difference pattern further uncovers the electron transfers from the anionic polysulfide and sulfonate to the cationic imidazole and Li^+ , respectively (Figure S4). These results are highly consistent with the above spectral characterizations, which evidentially describe the interaction mechanism between the as-developed zwitterion and LiPS. In addition, the geometrically stable configurations, electron distributions, electron density differences and binding energies between MIPS and other soluble LiPS, i.e., Li_2S_6 and Li_2S_8 , are also presented in Figure S5, which demonstrate the good commonality of the PZI-LiPS interactions upon the Li-S battery chemistry. When employed as interlayer in battery configuration, these interactions are expected to rigidly anchor the early-leached polysulfides and establish a high-concentration barrier against the penetration of subsequent polysulfides, while simultaneously offering a favorable Li^+ conduction. Consequently, a desirable polysulfide regulation can be implemented to overcome the stubborn shuttle issue while retaining the intriguing merits of solution-based sulfur electrochemistry.

1
2
3 **Polysulfide obstruction and Li⁺ conduction.** For a proof-of-concept, the PZI interlayer
4 was constructed via the direct polymerization on conventional polypropylene-based
5 separator (denoted as PZI@PP). As shown in Figure 4a, the scanning electron microscope
6 (SEM) image of pristine PP membrane shows a typical porous surface. By contrast, a
7 smooth and non-porous surface can be observed for the PZI@PP membrane, suggesting
8 the good spreading of dense PZI layer (Figure 4b). Further surface characterization reveals
9 a smaller contact angle of 14.5° for electrolyte drop on PZI@PP than that on pristine PP
10 (26.3°) membrane (Figure 4a-b, bottom), indicating the superior affinity of PZI to
11 electrolyte, which is favorable to the electrolyte infiltration and Li⁺ transfer. The backside
12 of PZI@PP separator remains the porous surface, suggesting the mainly one-side coating
13 (Figure S6). The cross-section observation in Figure 4c determines the ultrathin PZI layer
14 of ~0.2 μm (mass loading: ca. 0.434 mg cm⁻²; the authentic PZI thickness could be slightly
15 larger due to the partial precursor infiltration in PP separator), which is intentionally
16 controlled under multiple considerations including i) lowering the absolute resistance for
17 Li⁺ transfer, ii) minimizing the active sulfur loss by adsorption and iii) reducing the offset
18 in energy density at cell level. In order to examine the polysulfide regulation, the PZI@PP
19 membrane was subject to a visual simulation of polysulfide diffusion, where LiPS solution
20 (0.2 M Li₂S₄/DME+DOL) and blank solvent were separated by PP or PZI@PP membrane
21 in a H-type cell (Figure 4d). It should be noted that the relatively high LiPS concentration
22 and low PZI loading were employed to neglect the color variation induced by direct LiPS
23 entrapment in PZI. With pristine PP separator, the opposite chamber witnesses a distinct
24 change from colorless to light orange after 6 h, and further into dark brown after 48 h,
25 signifying that polysulfide species can easily diffuse through the porous separator and give
26 rise to serious shuttle effect in the corresponding Li-S cells. By contrast, the as-developed
27 PZI@PP separator enables a clear and colorless solution even after 48 h, confirming its
28 great capability of blocking polysulfide diffusion. Such excellent polysulfide obstruction
29 originates from the strong chemical interactions between PZI and LiPS as evidenced above,
30 which immobilizes LiPS and establishes a robust barrier against the subsequent polysulfide
31 penetration. This admirable feature is expected to effectively inhibit the shuttling behaviors
32 and stabilize the Li-S battery chemistry.
33
34
35
36
37
38
39
40
41
42
43
44
45
46
47
48
49
50
51
52
53
54
55
56
57
58
59
60

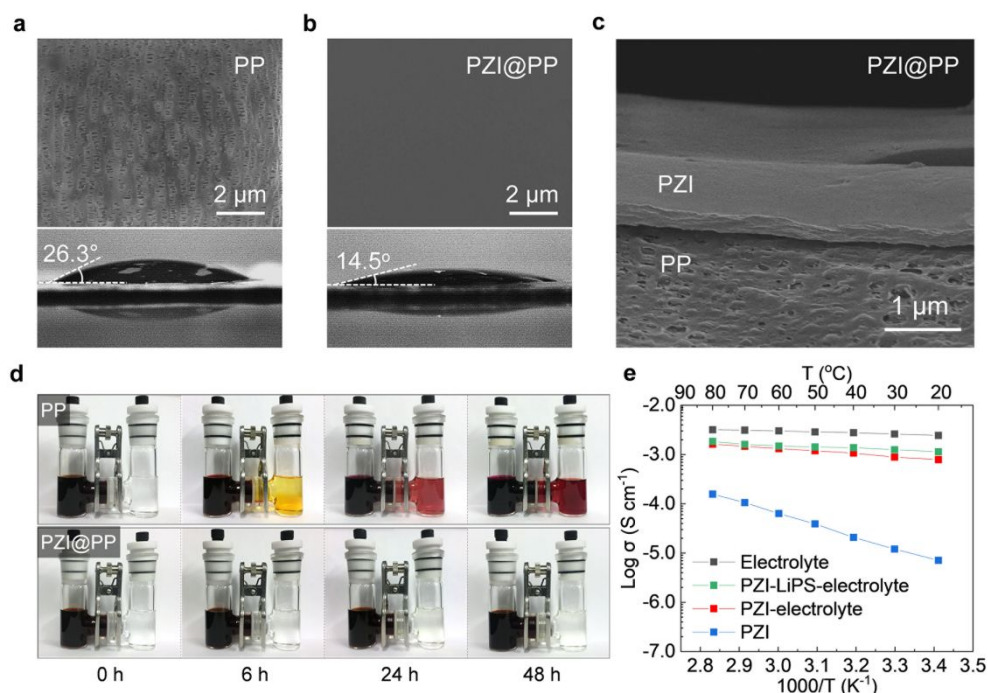


Figure 4. Top-view SEM images and electrolyte contact angles on (a) PP and (b) PZI@PP membranes; (c) cross-section image of PZI@PP membrane; (d) polysulfide diffusion comparison in H-type cells with PP and PZI@PP separators; (e) ionic conductivities of neat PZI, PZI in electrolyte and PZI in LiPS-contained electrolyte.

Apart from polysulfide blockage, Li^+ conduction property is another criterion for rational interlayer construction in Li-S batteries. Eligible polysulfide obstruction need be established without sacrificing the Li^+ conductivity to guarantee a decent sulfur reaction kinetics. In view of this, the Li^+ conduction within the PZI matrix was investigated in different conditions as shown in Figure 4e. The as-developed PZI delivers a fair intrinsic conductivity of $1.21 \times 10^{-5} \text{ S cm}^{-1}$ at 30 °C due to the strong dipolar interaction between $-\text{SO}_3^-$ and Li^+ , high donor number of ethoxy unit to Li^+ , and decent Li^+ solvation by the lean DEM/DOL incorporated in the matrix. After fully soaked by electrolyte, PZI exhibits a significantly enhanced conductivity up to $8.89 \times 10^{-4} \text{ S cm}^{-1}$ (30 °C), which is close to that of pure electrolyte, confirming its good electrolyte wettability and facile Li^+ permission. Apart from that, the Li^+ conduction in PZI was further examined in LiPS-contained (0.2 M Li_2S_4) electrolyte to simulate the condition upon battery operation. The result shows an even higher conductivity of $1.26 \times 10^{-3} \text{ S cm}^{-1}$ (30 °C), manifesting the expedite Li^+ transfer

1
2
3 after LiPS adsorption, which favors the facile and stable sulfur reactions combined with a
4 strong polysulfide regulation. Beyond that, this desirable combination in PZI was further
5 characterized by Li^+ transference number (t_{Li^+}), which was measured in 0.2 M
6 $\text{Li}_2\text{S}_4/(\text{DME}+\text{DOL})$ electrolyte with lithium foil as symmetric electrodes. Based on the
7 chronoamperometry (CA) and electrochemical impedance spectroscopy (EIS) results
8 (Figure S7), a favorably higher t_{Li^+} ca. 0.94 can be achieved for PZI@PP compared with
9 that of pristine PP separator (ca. 0.59), confirming the great capability of PZI in blocking
10 polysulfide permeation while simultaneously allowing fast Li^+ transfer. Such ionic sieve is
11 expected to efficiently inhibit the shuttle effect and retain a fast sulfur reaction kinetics.
12
13
14
15
16
17
18
19

20 **Electrochemistry of PZI-based Li-S batteries.** In view of the above results, the as-
21 developed PZI@PP separator was implemented in Li-S coin cells to examine its practical
22 effects on battery performance. Simple sulfur/carbon (S/C) composite was prepared as the
23 cathode active material (see details in Experimental). SEM observation and element
24 mapping confirm the uniform sulfur distribution in the composite (Figure S8). The sulfur
25 content was determined ca. 79.8 wt.% by TGA as shown in Figure S9. Additionally, the
26 electrochemical stability of PZI was verified before the battery evaluation as shown in
27 Figure S10. The CV profile clearly reveals the good electrochemical stability of PZI,
28 showing negligible current response within the potential range of 1.5 to 3.0 V (vs. Li/Li^+ ,
29 hereafter inclusive), which covers the voltage range for regular Li-S battery operation.
30 Additionally, the linear sweep voltammetry (LSV) signifies the relatively extended
31 oxidative and reductive limits for PZI-electrolyte, demonstrating the good electrochemical
32 stability of the electrolyte system (Figure S11). Figure 5a depicts the galvanostatic charge-
33 discharge profiles of Li-S cell with PZI@PP separator. A typical two-plateau discharge
34 curve can be observed. The upper plateau at 2.35 V corresponds to the reduction of element
35 sulfur into long-chain soluble LiPS (Li_2S_n , $4 \leq n \leq 8$), while the lower plateau at 2.1 V is
36 assigned to further sulfur reduction into insoluble $\text{Li}_2\text{S}_2/\text{Li}_2\text{S}$.⁴⁶ A considerable capacity
37 decrease can be perceived from 1st to 2nd cycle, which could be ascribed to the sulfur loss
38 by LiPS dissolution as well as their adsorption by the PZI interlayer. However, subsequent
39 fading was effectively retarded with high capacity retention at 200th and 300th cycles. It is
40 also worth noting that the voltage profile well maintains upon 300 cycles with negligible
41
42
43
44
45
46
47
48
49
50
51
52
53
54
55
56
57
58
59
60

1
2
3 polarization aggravation, indicating the good reaction kinetics and stabile sulfur
4 electrochemistry.
5
6
7

8 The CV result echoes well with the voltage profile, showing two cathodic peaks and an
9 overlapped anodic peak as presented in Figure 5b. Similarly, the CV curves witness a
10 declined current response at 2nd cycle, but well maintains the profile upon the initial several
11 cycles, suggesting a favorable electrochemical reversibility. Cycling performance was
12 compared between cells with pristine PP and PZI@PP separators at C/5 rate (1C=1675 mA
13 g⁻¹) as shown in Figure 5c. The PZI@PP cell shows an initial capacity of 1279.6 mAh g⁻¹,
14 which decreases to 1095.6 mAh g⁻¹ at 2nd cycle due to the LiPS dissolution in electrolyte
15 and adsorption by PZI. After that, the capacity stabilizes and maintains at 1031.3 mAh g⁻¹
16 after 300 cycles. In comparison, the PP cell shows relatively higher capacity than that with
17 PZI@PP at initial several cycles, which could be attributed to, on the one hand, the
18 relatively higher Li⁺ conductivity of pure electrolyte as reflected by the smaller
19 electrochemical resistance (Figure S12). On the other hand, the absence of sulfur loss by
20 PZI adsorption also partially contributes to the slower capacity fading at initial stage.
21 Nevertheless, the PP-based cell suffers from continuous capacity degradation to 808.2 mAh
22 g⁻¹ at 100th cycle, presenting a drastic contrast to the stable cycling behavior in PZI-based
23 configuration. The significant enhancement of cell cyclability benefits from the as-
24 constructed PZI interlayer, which establishes, despite a slight sulfur sacrifice, a highly
25 effective polysulfide barrier against their penetration, thus constraining the active species
26 within the cathode to be efficiently utilized instead of being continuously consumed by the
27 shuttle effect.
28
29
30
31
32
33
34
35
36
37
38
39
40
41
42
43
44
45
46
47
48
49
50
51
52
53
54
55
56
57
58
59
60

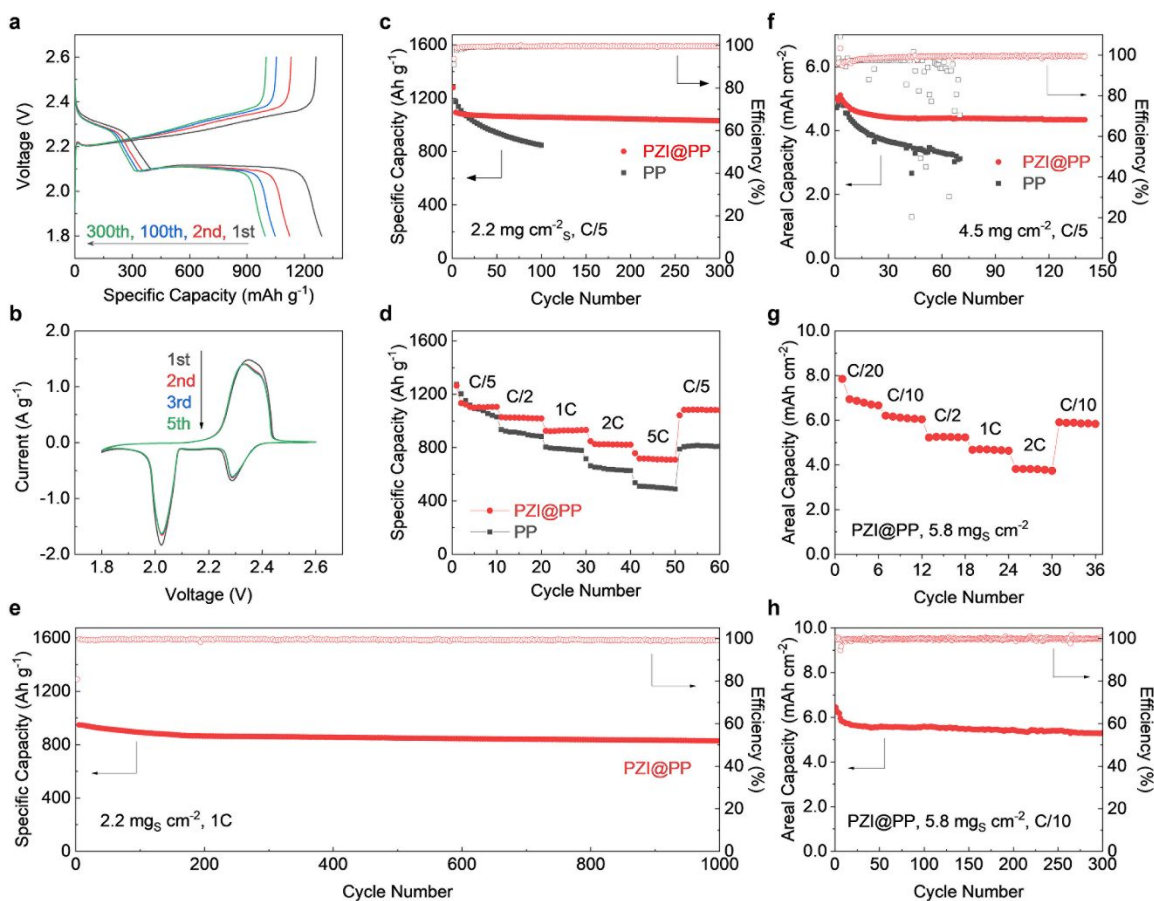


Figure 5. (a) Voltage profiles and (b) CV curves of PZI@PP cells at different cycles; (c) cycling comparison between PP and PZI@PP cells at C/5 under sulfur loading of 2.2 mg cm^{-2} ; (d) voltage profiles of PZI@PP cell at different current rates; (e) multi-rate performance comparison between PP and PZI@PP cells; (f) long-term cycling performance of PZI@PP cell at 1C; (g) cycling comparison between PP and PZI@PP cells at C/5 under sulfur loading of 4.5 mg cm^{-2} ; (h) prolonged cycling performance of PZI@PP cell at C/10 under sulfur loading of 5.8 mg cm^{-2} .

To understand the cyclability improvement by PZI interlayer, in situ UV-vis spectra were collected upon the first discharge in H-type cells with different separators. The absorbances at 330 and 430 nm^{-1} were highlighted as typical responses of LiPS in UV-vis spectra.^{47,48} As shown in Figure S13, these responses in cathode chamber undergo similar evolution along with the depth of discharge (DOD) in PP and PZI@PP cells, conforming to the variation of LiPS concentration in electrolyte. This indicates the similar cathode reaction behaviors in these two configurations. Whereas in anode chamber, PZI@PP separator

1
2
3 enables a consistently negligible absorbance in distinct comparison with the continuous
4 LiPS increase in PP-based cell, strongly validating the effective sulfur confinement by PZI
5 interlayer upon the practical Li-S battery operation. Moreover, the EIS variations upon the
6 cycling were also recorded as shown in Figure S14. The typical Nyquist plot of cycled Li-S
7 cell shows two suppressed semicircles at high and medium frequency ranges, which are
8 assigned to the interfacial (R_{int}) and charge transfer (R_{ct}) resistances, respectively. The
9 intercept at real axis corresponds to the solution resistance (R_{s}), while the slope at low
10 frequency presents the Warburg resistance.⁴⁹ It can be clearly noticed that the PZI@PP
11 separator enables a more stable and lower resistances for all the R_{s} , R_{int} and R_{ct} upon the
12 cycling, manifesting the facilitated and stabilized sulfur electrochemistry attributed to the
13 rational polysulfide regulation.
14
15
16
17
18
19
20
21
22
23

24 The effective shuttle inhibition was further determined by the cycling comparison in
25 electrolyte without LiNO_3 . Generally, LiNO_3 is a classic electrolyte additive which forms
26 robust and protective solid electrolyte interphase (SEI) layer on anode surface against the
27 detrimental attacks from polysulfides.⁵⁰ Hence, the cycling behavior without LiNO_3 is a
28 well-acknowledged indicator of shuttle severity in Li-S cells. As shown in Figure S15a,
29 PZI@PP enables superior cyclability with higher capacity retention, and more importantly,
30 higher and more stable coulombic efficiency than those with PP separator over 50 cycles.
31 In addition, a significantly smaller shuttle current can be also obtained for PZI@PP cell,
32 which strongly confirms its significant inhibition on shuttle effect (Figure S15b). Apart
33 from that, post-mortem SEM and Energy Dispersive X-ray Spectroscopy (EDX) was
34 performed on anode surface to further study the shuttling behavior in different
35 configurations. As shown in Figure S16, the Li surface with PZI@PP separator shows
36 comparatively an intact and smooth surface, while apparent cracks and dendrites can be
37 observed for that with PP separator. In addition, the EDX spectrum reveals a lower sulfur
38 content on Li surface in PZI@PP cell, manifesting the limited detrimental reactions from
39 shuttle effect (Figure S17). Moreover, the PZI@PP separator delivers an orange round spot
40 at cathodic side in contrast to the both clean and white sides of pristine PP separator after
41 cycling and washing by DME/DOL, further demonstrating the significantly stronger sulfur
42 immobilization by PZI (Figure S18). Furthermore, as another important shuttle indicator,
43
44
45
46
47
48
49
50
51
52
53
54
55
56
57
58
59
60

1
2
3 the self-discharge behavior was also examined for different cells. As shown in Figure S19a,
4 the PZI@PP cell exhibits a significantly higher and steadier open circuit voltage (OCV)
5 compared with its PP counterpart upon 72 h resting after 5 pre-cycles. This confirms the
6 excellent polysulfide obstruction by PZI barrier, which limits the polysulfide accessibility
7 to Li anode and their direct reactions, thus mitigating the voltage degradation and the
8 irreversible capacity loss as revealed in Figure S19b and c. All these results consistently
9 demonstrate the excellent suppression of polysulfide shuttling and the stabilization of
10 sulfur electrochemistry by the as-constructed PZI barrier.
11
12
13
14
15
16
17
18

19 The rate performances of different cells were also examined as presented in Figure 5d. The
20 PP cell suffers from a serious capacity degradation along with the increase of current rate,
21 resulting in a capacity of 510.8 mAh g⁻¹ at 5 C. By contrast, the PZI@PP separator fulfills
22 a good rate capability with a high capacity of 718.4 mAh g⁻¹ at 5 C, which recovers to
23 1082.9 mAh g⁻¹ as switched back to C/2, manifesting the highly reversible and expedite
24 sulfur redox reactions. The kinetic virtue also gains strong support from the voltage profiles
25 at different rates, where the discharge curve well maintains the two-plateau profile even at
26 a high rate up to 5 C (Figure S20). Given the above results, a long-term cycling evaluation
27 was conducted for PZI@PP cell at 1 C as shown in Figure 5f. A favorable capacity retention
28 of 828.5 mAh g⁻¹ can be maintained after a prolonged 1000 cycles, corresponding to a
29 minimum capacity fading rate of 0.012 % per cycle since the 2nd cycle. It should be noted
30 that these electrochemical performances are highly competitive among the recent
31 literatures with various separator engineering (Table S1). These results strongly illustrate
32 the great superiority of PZI in facilitating and stabilizing sulfur electrochemistry towards
33 high-performance Li-S batteries.
34
35
36
37
38
39
40
41
42
43
44
45

46 To explore the practical viability of the as-developed PZI@PP separator, raised sulfur
47 loadings were implemented to examine the regulation effect under polysulfide-flooding
48 condition as well as pursuing higher energy density. Figure 5g presents the cycling
49 comparison between high-loading sulfur electrodes (4.5 mg_S cm⁻²) with different separators.
50 Contrastively, PZI@PP enables a much higher areal capacity retention of 4.0 mAh cm⁻²
51 after 140 cycles. More importantly, the PZI@PP cell maintains a high and stable coulombic
52
53
54
55
56
57
58
59
60

1
2
3 efficiency upon the cycling, whereas the PP counterpart suffers from low and fluctuant
4 efficiency ascribed to the riotous polysulfide shuttling. This distinct comparison strongly
5 confirms the highly effective polysulfide regulation by PZI even under a high-loading
6 configuration. In addition, varied sulfur loadings and electrolyte to sulfur (E/S, mL g⁻¹_S)
7 ratios were investigated for PZI-based cells. Generally, highest possible sulfur loading and
8 lowest possible E/S ratio are desired in pursuit of high energy density at cell level, whereas
9 the practical implementation is always frustrated by the consequent deteriorations in sulfur
10 utilization and reaction kinetics.⁵¹ As shown in Figure S21, a continuous enhancement in
11 areal capacity can be obtained along with the increase of sulfur loading, although some
12 level of degradation in sulfur utilization and cycling stability can be perceived ascribed to
13 the increasing challenges regarding the mechanical integrity and electron/ion transfer.⁵²
14 But still, a high areal capacity of 7.85 mAh cm⁻² can be obtained under a raised sulfur
15 loading up to 8.2 mg cm⁻², demonstrating that a decent sulfur electrochemistry is available
16 even under high sulfur loading in the PZI-based configuration.
17
18
19
20
21
22
23
24
25
26
27
28

29 Figure S22 depicts the discharge profiles and cycling performances of PZI@PP cells under
30 different E/S ratios. As a delicate but critical index in solution-based Li-S battery chemistry,
31 E/S ratio requires to be rationally managed to ensure facile sulfur conversions while
32 retaining high energy density at cell level. It can be perceived that a clear two-plateau
33 discharge profile can be still achievable at a low E/S ratio of 3, indicating the decent
34 reaction kinetics even with relatively lean electrolyte. However, continuous reduction of
35 both the discharge plateau potential and areal capacity can be also observed along with the
36 decrease of E/S ratio, signifying the aggravation of electrochemical polarization and
37 reaction resistance induced by the increase of polysulfide concentration, degradation of
38 electrolyte conductivity, limited sulfur solid-liquid phase conversion, etc.^{53,54} Based on
39 these results, a modest sulfur loading of 5.8 mg cm⁻² and E/S ratio of 7 were employed for
40 rate and prolonged cycling evaluation. The result shows considerable capacity of 3.82 mAh
41 cm⁻² and well-maintained multi-stage profile under a high rate up to 2 C, confirming the
42 decent reaction kinetics in PZI-based high-loading configuration (Figure 5g and Figure
43 S23). Meanwhile, the PZI@PP cell also exhibits an excellent cycling stability with a high
44 capacity of 5.3 mAh cm⁻² after 300 cycles corresponding to a favorable capacity retention
45
46
47
48
49
50
51
52
53
54
55
56
57
58
59
60

1
2
3 of 82.2 % (Figure 5h). Besides, a constantly high coulombic efficiency can be maintained
4 over the cycling, indicating the efficient and stable sulfur electrochemistry attributed to the
5 rational polysulfide regulation. These results are also highly competitive among the
6 recently reported high-loading performances based on interlayer designs (Table S2), which
7 further demonstrates the intriguing potential of the as-developed PZI interlayer in pursuit
8 of high-performance and practically-viable Li-S batteries.
9
10
11
12
13
14

15 **CONCLUSIONS**

16
17 In summary, a unique polymeric zwitterion was developed for rational polysulfide
18 regulation towards high-energy and durable Li-S batteries. The as-developed PZI
19 covalently anchors the sulfophilic and lithiophilic sites in the polymeric framework,
20 empowering strong polysulfide immobilization and facile Li⁺ conduction simultaneously.
21 When implemented as interlayer in Li-S configuration, PZI establishes a robust polysulfide
22 barrier that selectively obstructs the polysulfide penetration while allowing decent Li⁺
23 transfer through the separator, thus contributing to inhibited shuttle effect and stabilized
24 Li-S battery chemistry. Benefiting from these attributes, significantly improved cyclability
25 over 1000 cycles and rate capability up to 5 C can be achieved for simple S/C composite
26 electrode. Moreover, commendable areal capacity and cycling stability are also accessible
27 under high sulfur loading and limited electrolyte. This work paves a new pathway toward
28 rational polysulfide regulation and highly stable solution-based sulfur electrochemistry,
29 holding a great promise in promoting the future development of practical Li-S batteries.
30
31
32
33
34
35
36
37
38
39
40
41
42

43 **ASSOCIATED CONTENT**

44 **Supporting Information**

45
46 Experimental details and supplemental physicochemical, electrochemical and
47 computational results (FTIR, TGA, DSC, EIS, UV-vis, etc.) data are included within SI.
48 This material is available free of charge via the Internet at <http://XXXX>.
49
50
51
52

53 **AUTHOR INFORMATION**

54 **Corresponding Authors**

55
56
57
58
59
60

1
2
3 zhwchen@uwaterloo.ca

4
5 wangxin@scnu.edu.cn

6
7
8 **Notes**

9
10 The authors declare no competing financial interest.

11
12
13 **ACKNOWLEDGEMENTS**

14
15 The authors would like to acknowledge the financial support from the Natural Sciences
16 and Engineering Research Council of Canada (NSERC), National Natural Science
17 Foundation of China Program (No. 51602111), Xijiang R&D Team (X. W.) and University
18 of Waterloo.
19
20
21
22
23

24 **REFERENCE**

- 25
26
27 (1) Dunn, B.; Kamath, H.; Tarascon, J. M., Electrical energy storage for the grid: a battery of
28 choices. *Science* **2011**, *334*, 928.
29 (2) Bruce, P. G.; Freunberger, S. A.; Hardwick, L. J.; Tarascon, J. M., Li-O₂ and Li-S batteries
30 with high energy storage. *Nat. Mater.* **2011**, *11*, 19.
31 (3) Cano, Z. P.; Banham, D.; Ye, S. Y.; Hintennach, A.; Lu, J.; Fowler, M.; Chen, Z. W.,
32 Batteries and fuel cells for emerging electric vehicle markets. *Nat. Energy* **2018**, *3*, 279.
33 (4) Manthiram, A.; Fu, Y. Z.; Chung, S. H.; Zu, C. X.; Su, Y. S., Rechargeable lithium-sulfur
34 batteries. *Chem. Rev.* **2014**, *114*, 11751.
35 (5) Ji, X. L.; Lee, K. T.; Nazar, L. F., A highly ordered nanostructured carbon-sulphur cathode
36 for lithium-sulphur batteries. *Nat. Mater.* **2009**, *8*, 500.
37 (6) Yin, Y. X.; Xin, S.; Guo, Y. G.; Wan, L. J., Lithium-sulfur batteries: electrochemistry,
38 materials, and prospects. *Angew. Chem. Int. Ed. Engl.* **2013**, *52*, 13186.
39 (7) Lang, S. Y.; Xiao, R. J.; Gu, L.; Guo, Y. G.; Wen, R.; Wan, L. J., Interfacial Mechanism
40 in Lithium-Sulfur Batteries: How Salts Mediate the Structure Evolution and Dynamics. *J. Am.*
41 *Chem. Soc.* **2018**, *140*, 8147.
42 (8) Zhang, J.; Yang, C. P.; Yin, Y. X.; Wan, L. J.; Guo, Y. G., Sulfur encapsulated in graphitic
43 carbon nanocages for high-rate and long-cycle lithium-sulfur batteries. *Adv. Mater.* **2016**, *28*, 9539.
44 (9) Xin, S.; Gu, L.; Zhao, N. H.; Yin, Y. X.; Zhou, L. J.; Guo, Y. G.; Wan, L. J., Smaller sulfur
45 molecules promise better lithium-sulfur batteries. *J. Am. Chem. Soc.* **2012**, *134*, 18510.
46 (10) Han, F. D.; Yue, J.; Fan, X. L.; Gao, T.; Luo, C.; Ma, Z. H.; Suo, L. M.; Wang, C. S., High-
47 performance all-solid-state lithium-sulfur battery enabled by a mixed-conductive Li₂S
48 nanocomposite. *Nano Lett.* **2016**, *16*, 4521.
49 (11) Wei, S. Y.; Ma, L.; Hendrickson, K. E.; Tu, Z. Y.; Archer, L. A., Metal-sulfur battery
50 cathodes based on PAN sulfur composites. *J. Am. Chem. Soc.* **2015**, *137*, 12143.
51 (12) Manthiram, A.; Yu, X. W.; Wang, S. F., Lithium battery chemistries enabled by solid-state
52 electrolytes. *Nat. Rev. Mater.* **2017**, *2*, 16103.
53 (13) Guo, J. C.; Yang, Z. C.; Yu, Y. C.; Abruna, H. D.; Archer, L. A., Lithium-Sulfur Battery
54 Cathode Enabled by Lithium-Nitrile Interaction. *J. Am. Chem. Soc.* **2013**, *135*, 763.
55
56
57

- 1
2
3 (14) Li, G. R.; Wang, S.; Zhang, Y. N.; Li, M.; Chen, Z. W.; Lu, J., Revisiting the role of
4 polysulfides in lithium-sulfur batteries. *Adv. Mater.* **2018**, *30*, 1705590.
- 5 (15) Peng, H. J.; Huang, J. Q.; Liu, X. Y.; Cheng, X. B.; Xu, W. T.; Zhao, C. Z.; Wei, F.; Zhang,
6 Q., Healing High-Loading Sulfur Electrodes with Unprecedented Long Cycling Life: Spatial
7 Heterogeneity Control. *J. Am. Chem. Soc.* **2017**, *139*, 8458.
- 8 (16) Liu, F.-Q.; Wang, W.-P.; Yin, Y.-X.; Zhang, S.-F.; Shi, J.-L.; Wang, L.; Zhang, X.-D.;
9 Zheng, Y.; Zhou, J.-J.; Li, L., Upgrading traditional liquid electrolyte via in situ gelation for future
10 lithium metal batteries. *Sci. Adv.* **2018**, *4*, eaat5383.
- 11 (17) Mao, Y. Y.; Li, G. R.; Guo, Y.; Li, Z. P.; Liang, C. D.; Peng, X. S.; Lin, Z., Foldable
12 interpenetrated metal-organic frameworks/carbon nanotubes thin film for lithium-sulfur batteries.
13 *Nat. Commun.* **2017**, *8*, 14628.
- 14 (18) Yang, Y.; Zheng, G. Y.; Cui, Y., A membrane-free lithium/polysulfide semi-liquid battery
15 for large-scale energy storage. *Energy Environ. Sci.* **2013**, *6*, 1552.
- 16 (19) Chen, S. R.; Dai, F.; Gordin, M. L.; Yu, Z. X.; Gao, Y.; Song, J. X.; Wang, D. H.,
17 Functional organosulfide electrolyte promotes an alternate reaction pathway to achieve high
18 performance in lithium-sulfur batteries. *Angew. Chem., Int. Ed.* **2016**, *55*, 4231.
- 19 (20) Fan, L. L.; Li, M.; Li, X. F.; Xiao, W.; Chen, Z. W.; Lu, J., Interlayer material selection
20 for lithium-sulfur batteries. *Joule* **2019**, *3*, 361.
- 21 (21) Huang, J. Q.; Zhang, Q.; Wei, F., Multi-functional separator/interlayer system for high-
22 stable lithium-sulfur batteries: Progress and prospects. *Energy Storage Mater.* **2015**, *1*, 127.
- 23 (22) Lei, T. Y.; Chen, W.; Lv, W. Q.; Huang, J. W.; Zhu, J.; Chu, J. W.; Yan, C. Y.; Wu, C. Y.;
24 Yan, Y. C.; He, W. D.; Xiong, J.; Li, Y. R.; Yan, C. L.; Goodenough, J. B.; Duan, X. F., Inhibiting
25 polysulfide shuttling with a graphene composite separator for highly robust lithium-sulfur batteries.
26 *Joule* **2018**, *2*, 2091.
- 27 (23) Li, X.; Sun, X. L., Interface design and development of coating materials in lithium-sulfur
28 batteries. *Adv. Funct. Mater.* **2018**, *28*, 1801323.
- 29 (24) Cai, W. L.; Li, G. R.; Zhang, K. L.; Xiao, G. N.; Wang, C.; Ye, K. F.; Chen, Z. W.; Zhu,
30 Y. C.; Qian, Y. T., Conductive nanocrystalline niobium carbide as high-efficiency polysulfides
31 tamer for lithium-sulfur batteries. *Adv. Funct. Mater.* **2018**, *28*, 1704865.
- 32 (25) Huang, J. Q.; Zhang, Q.; Peng, H. J.; Liu, X. Y.; Qian, W. Z.; Wei, F., Ionic shield for
33 polysulfides towards highly-stable lithium-sulfur batteries. *Energy Environ. Sci.* **2014**, *7*, 347.
- 34 (26) He, Y.; Qiao, Y.; Chang, Z.; Cao, X.; Jia, M.; He, P.; Zhou, H., Developing a
35 “polysulfide-phobic” strategy to restrain shuttle effect in lithium-sulfur batteries. *Angew. Chem.*
36 **2019**, *58*, 11774.
- 37 (27) Lu, F.; Gao, X. P.; Doug, B.; Sun, P. P.; Sun, N.; Xie, S. T.; Zheng, L. Q., Nanostructured
38 proton conductors formed via in situ polymerization of ionic liquid crystals. *ACS Appl. Mater. Inter.*
39 **2014**, *6*, 21970.
- 40 (28) Lu, F.; Gao, X. P.; Wu, A. L.; Sun, N.; Shi, L. J.; Zheng, L. Q., Lithium-containing
41 zwitterionic poly(Ionic liquid)s as polymer electrolytes for lithium-ion batteries. *J. Phys. Chem. C*
42 **2017**, *121*, 17756.
- 43 (29) Hoag, B. P.; Gin, D. L., Cross-linkable liquid crystal monomers containing hydrocarbon
44 1,3-diene tail systems. *Macromolecules* **2000**, *33*, 8549.
- 45 (30) Rahman, M. T.; Barikbin, Z.; Badruddoza, A. Z. M.; Doyle, P. S.; Khan, S. A.,
46 Monodisperse polymeric ionic liquid microgel beads with multiple chemically switchable
47 functionalities. *Langmuir* **2013**, *29*, 9535.
- 48 (31) Ma, Q.; Zhang, H.; Zhou, C. W.; Zheng, L. P.; Cheng, P. F.; Nie, J.; Feng, W. F.; Hu, Y.
49 S.; Li, H.; Huang, X. J.; Chen, L. Q.; Armand, M.; Zhou, Z. B., Single lithium-ion conducting
50 polymer electrolytes based on a super-delocalized polyanion. *Angew. Chem., Int. Ed.* **2016**, *55*,
51 2521.
52
53
54
55
56
57
58
59
60

- (32) Zhang, H.; Li, C. M.; Piszcz, M.; Coya, E.; Rojo, T.; Rodriguez-Martinez, L. M.; Armand, M.; Zhou, Z. B., Single lithium-ion conducting solid polymer electrolytes: advances and perspectives. *Chem. Soc. Rev.* **2017**, *46*, 797.
- (33) Ohno, H.; Yoshizawa-Fujita, M.; Kohno, Y., Design and properties of functional zwitterions derived from ionic liquids. *Phys. Chem. Chem. Phys.* **2018**, *20*, 10978.
- (34) Islam, A.; Li, J. G.; Pervaiz, M.; Lu, Z. H.; Sain, M.; Chen, L. H.; Ouyang, X. H., Zwitterions for organic/perovskite solar cells, light-emitting devices, and lithium ion batteries: recent progress and perspectives. *Adv. Energy Mater.* **2019**, *9*, 1803354.
- (35) Handy, S. T.; Okello, M., The 2-position of imidazolium ionic liquids: Substitution and exchange. *J. Org. Chem.* **2005**, *70*, 1915.
- (36) Shi, L. J.; Li, N.; Yan, H.; Gao, Y. A.; Zheng, L. Q., Aggregation behavior of long-chain N-aryl imidazolium bromide in aqueous solution. *Langmuir* **2011**, *27*, 1618.
- (37) Hou, T. Z.; Xu, W. T.; Chen, X.; Peng, H. J.; Huang, J. Q.; Zhang, Q., Lithium bond chemistry in lithium-sulfur batteries. *Angew. Chem., Int. Ed.* **2017**, *56*, 8178.
- (38) Soberats, B.; Yoshio, M.; Ichikawa, T.; Ohno, H.; Kato, T., Zwitterionic liquid crystals as 1D and 3D lithium ion transport media. *J. Mater. Chem. A* **2015**, *3*, 11232.
- (39) Yu, Y.; Lu, F.; Sun, N.; Wu, A. L.; Pan, W.; Zheng, L. Q., Single lithium-ion polymer electrolytes based on poly(ionic liquid)s for lithium-ion batteries. *Soft Matter* **2018**, *14*, 6313.
- (40) Berthomieu, C.; Boussac, A., FTIR and EPR study of radicals of aromatic-amino-acids 4-methylimidazole and phenol generated by UV irradiation. *Biospectroscopy* **1995**, *1*, 187.
- (41) Mao, H.; Song, Y.; Qian, D. M.; Liu, D. L.; Wu, S. Y.; Zhang, Y.; Hisaeda, Y.; Song, X. M., One-step preparation of flower-like poly(styrene-co-zwitterionic ionic liquid) microspheres with hierarchical structures for supported acidic heterogeneous catalysts. *RSC Adv.* **2015**, *5*, 91654.
- (42) Steinruck, H. P., Recent developments in the study of ionic liquid interfaces using X-ray photoelectron spectroscopy and potential future directions. *Phys. Chem. Chem. Phys.* **2012**, *14*, 5010.
- (43) Li, G. R.; Lei, W.; Luo, D.; Deng, Y. P.; Wang, D. L.; Chen, Z. W., 3D porous carbon sheets with multidirectional ion pathways for fast and durable lithium-sulfur batteries. *Adv. Energy Mater.* **2018**, *8*, 1702381.
- (44) Pang, Q.; Kundu, D.; Cuisinier, M.; Nazar, L. F., Surface-enhanced redox chemistry of polysulfides on a metallic and polar host for lithium-sulphur batteries. *Nat. Commun.* **2014**, *5*, 4759.
- (45) Liang, X.; Hart, C.; Pang, Q.; Garsuch, A.; Weiss, T.; Nazar, L. F., A highly efficient polysulfide mediator for lithium-sulfur batteries. *Nat. Commun.* **2015**, *6*, 5682.
- (46) Li, G. R.; Lei, W.; Luo, D.; Deng, Y. P.; Deng, Z. P.; Wang, D. L.; Yu, A. P.; Chen, Z. W., Stringed "tube on cube" nanohybrids as compact cathode matrix for high-loading and lean-electrolyte lithium-sulfur batteries. *Energy Environ. Sci.* **2018**, *11*, 2372.
- (47) Zou, Q. L.; Lu, Y. C., Solvent-dictated lithium sulfur redox reactions: an operando UV-vis spectroscopic study. *J. Phys. Chem. Lett.* **2016**, *7*, 1518.
- (48) Chen, T.; Zhang, Z. W.; Cheng, B. R.; Chen, R. P.; Hu, Y.; Ma, L. B.; Zhu, G. Y.; Liu, J.; Jin, Z., Self-Templated Formation of Interlaced Carbon Nanotubes Threaded Hollow Co₃S₄ Nanoboxes for High-Rate and Heat-Resistant Lithium-Sulfur Batteries. *J. Am. Chem. Soc.* **2017**, *139*, 12710.
- (49) Deng, Z. F.; Zhang, Z. A.; Lai, Y. Q.; Liu, J.; Li, J.; Liu, Y. X., Electrochemical impedance spectroscopy study of a lithium/sulfur battery: modeling and analysis of capacity fading. *J. Electrochem. Soc.* **2013**, *160*, A553.
- (50) Zhang, S. S., Role of LiNO₃ in rechargeable lithium/sulfur battery. *Electrochim. Acta* **2012**, *70*, 344.
- (51) Hagen, M.; Hanselmann, D.; Ahlbrecht, K.; Maca, R.; Gerber, D.; Tubke, J., Lithium-sulfur cells: the gap between the state-of-the-art and the requirements for high energy battery cells. *Adv. Energy Mater.* **2015**, *5*, 1401986.

1
2
3 (52) Peng, H. J.; Huang, J. Q.; Cheng, X. B.; Zhang, Q., Review on high-loading and high-
4 energy lithium-sulfur batteries. *Adv. Energy Mater.* **2017**, *7*, 1700260.

5 (53) Chen, J. Z.; Henderson, W. A.; Pan, H. L.; Perdue, B. R.; Cao, R. G.; Hu, J. Z.; Wan, C.;
6 Han, K. S.; Mueller, K. T.; Zhang, J. G.; Shao, Y. Y.; Liu, J., Improving lithium-sulfur battery
7 performance under lean electrolyte through nanoscale confinement in soft swellable gels. *Nano Lett.*
8 **2017**, *17*, 3061.

9 (54) Yang, Y. X.; Zhong, Y. R.; Shi, Q. W.; Wang, Z. H.; Sun, K. N.; Wang, H. L.,
10 Electrocatalysis in lithium sulfur batteries under lean electrolyte conditions. *Angew. Chem., Int. Ed.*
11 **2018**, *57*, 15549.
12
13
14
15
16
17
18
19
20
21
22
23
24
25
26
27
28
29
30
31
32
33
34
35
36
37
38
39
40
41
42
43
44
45
46
47
48
49
50
51
52
53
54
55
56
57
58
59
60

TOC graphic

Polysulfide regulation by zwitterionic barrier towards durable lithium-sulfur batteries